resources

MDPI

Article

Microfluidic Study of Application of Nanosuspension with Aluminum Oxide Nanofibers to Enhance Oil Recovery Factor During Reservoir Flooding

Andrey Pryazhnikov [1], Vladimir Zhigarev [1,2], Maxim Pryazhnikov [1,2,*] and Andrey Minakov [1]

[1] Laboratory of Physical and Chemical Technologies for the Development of Hard-to-Recover Hydrocarbon Reserve, Siberian Federal University, Krasnoyarsk 660041, Russia; andron2793@yandex.ru (A.P.); zhigarev.vladimir@yandex.ru (V.Z.); tov-andrey@yandex.ru (A.M.)
[2] Department of Drilling of Oil and Gas Wells, Siberian Federal University, Krasnoyarsk 660041, Russia
* Correspondence: arrivent@yandex.ru

Abstract: The paper presents the results of a comparative microfluidic study of the oil displacement process from a microfluidic chip simulating rock. Suspensions of spherical nanoparticles of silicon oxide (22 nm) and aluminum oxide (11 nm), as well as aluminum oxide nanofibers (8.7 nm in diameter and with an aspect ratio of 58), were used as displacing liquids. The nanofibers represent a unique new-generation crystalline material with a high aspect ratio. This work presents the first consideration of the use of aluminum oxide nanofibers as an additive for enhanced oil recovery. The comparative analysis has demonstrated that the addition of nanofibers can markedly enhance the oil recovery factor relative to the addition of spherical nanoparticles, other things being equal. Thus, in particular, it was demonstrated that the addition of nanofibers into the system allows for the greatest enhancement of the oil recovery factor, reaching a value of 25%, whereas the addition of spherical nanoparticles results in a maximum increment of approximately 10%. This is due to the fact that nanofiber additives have a tenfold stronger effect on the viscosity of nanosuspensions compared to similar additives of spherical particles. Nanosuspensions of aluminum oxide nanofibers exhibit non-Newtonian behavior at low concentrations. This opens the possibility of their extensive use in enhanced oil recovery.

Keywords: enhanced oil recovery; microfluidics; porous medium; nanosuspension; nanofibers

check for updates

Citation: Pryazhnikov, A.; Zhigarev, V.; Pryazhnikov, M.; Minakov, A. Microfluidic Study of Application of Nanosuspension with Aluminum Oxide Nanofibers to Enhance Oil Recovery Factor During Reservoir Flooding. *Resources* **2024**, *13*, 160. https://doi.org/10.3390/resources13110160

Academic Editor: Benjamin McLellan

Received: 7 September 2024
Revised: 31 October 2024
Accepted: 1 November 2024
Published: 13 November 2024

Copyright: © 2024 by the authors. Licensee MDPI, Basel, Switzerland. This article is an open access article distributed under the terms and conditions of the Creative Commons Attribution (CC BY) license (https://creativecommons.org/licenses/by/4.0/).

1. Introduction

To date, the majority of large oil fields have reached the final stage of development. However, they still contain a considerable amount of residual recoverable oil reserves that have been accumulated in undeveloped areas or water flooded areas. A considerable proportion of the residual oil reserves in fields undergoing development are located in zones with low permeability, undersaturated oil reservoirs, and thin layers. The maintenance of oil production levels at such deposits is possible due to methodological studies and the development of recommendations on the optimization and improvement of the development system, targeted application of technologies, and oil recovery enhancement methods. Traditional methods of oil recovery enhancement include polymer, surfactant–polymer, and alkaline reservoir flooding [1,2]. However, the existing methods have a number of disadvantages, such as water tonguing breakthroughs in the case of polymer re-flooding immediately after the traditional reservoir flooding, the high cost of polymers, high degree polymer adsorption at the surface of the rock, and a number of other problems associated with reservoir conditions (high temperature, the degree of formation water mineralization). The use of surfactants–polymer–alkaline compositions is associated with a number of challenges, including the high cost of reagents and the initial costs associated with the preparation and pumping of these fluids during reservoir flooding [3]. At the present time, the advancement of displacement agent formulations has become a pivotal aspect in the oil

fields. Consequently, the methodological development of fields with challenging-to-recover reserves encompasses a system analysis of field development outcomes, an examination of prevailing, generally accepted methodologies, theoretical research, and the utilization of laboratory microfluidic studies for the selection of efficacious formulations and techniques for spot impact on the reservoir.

The article [4] presents a review of recent applications of microfluidics and microtechnology in the study of oil recovery and production processes. Microfluidic devices can be useful tools for the study and visualization of processes employed in the oil and gas industry, including fluid propagation, reservoir flooding, hydraulic fracturing, emulsification, and numerous others. A growing number of studies indicate that microfluidics is becoming, albeit slowly, a universally accepted methodology in this field.

In works [5], the authors proposed reservoir flooding as a potential method to enhance oil recovery from hydrophobic fractured rocks using surfactants. An experimental study was conducted using a microfluidic model. The authors [6] constructed micromodels with three porous structures and compared polymer and polymer–surfactant solutions to assess the effect of surfactants on pore-scale mobilization.

Nowadays, nanoparticle additives have been employed to enhance the properties of polymer and polymer–surfactant solutions. Recent studies have demonstrated the efficacy of nanoparticle-based formulations and suspensions in enhancing the efficiency of reservoir development in low-permeability and undersaturated reservoirs [7].

The authors of [8,9] have demonstrated the efficacy of utilizing displacement agents containing nanoparticles, which acted as microemulsion stabilizers. Furthermore, they have analyzed the collective impact of these agents on the displacement capacity of oil from the bulk model of a porous medium. Additionally, the works [10,11] illustrate the outcomes of nanoparticle application in the context of enhanced oil recovery. These studies demonstrate the impact of nanoparticle addition on the alteration of wettability, reduction of interfacial tension, enhancement of the viscosity of injected fluids, and prevention of asphaltene deposition.

Surfactant-stabilized nanoemulsions have the potential to be utilized in enhanced oil recovery operations for reservoirs with ultra-low permeability. In [10], the nanoemulsion for reservoir flooding demonstrates an ultra-low interfacial tension coefficient (less than 1×10^{-2} mN/m) and is capable of changing the core surface from hydrophobic to hydrophilic. Furthermore, it was observed that nanoemulsions with particle sizes ranging from 80 to 100 nm are capable of penetrating the small pores of reservoirs with ultra-low permeability.

In reservoir conditions, the performance of surfactants is enhanced due to the interaction between surfactants and nanofluids during reservoir flooding, which facilitates the production of hydrocarbons from conventional and unconventional shale reservoirs [12]. Numerous studies have demonstrated that nanoparticles exhibit enhanced resilience to unfavorable reservoir conditions [13,14]. Nanoparticles can form complexes with surfactants that adsorb at liquid–liquid and solid–liquid interfaces, thereby achieving a significant reduction of the oil–water interface and converting the rock to a more hydrophilic state than would be achieved with surfactant molecules alone [15,16]. Nanoparticles reduce the adsorption of surfactants on rock surfaces due to the adsorption of surfactant molecules between nanoparticles and rock surfaces and can increase the stability of surfactants in downhole conditions [17–19].

In our recent work [20], an experimental investigation was conducted to assess the impact of the weight concentration of silica nanoparticles with an average size of 22 nm on the oil recovery efficiency when pumping a displacement agent through a microchip made of glass. The microchip design permitted visual observations of the oil displacement process. As a result, nonlinear dependencies of breakthrough time and oil recovery factor on nanoparticle weight concentration were identified. It was demonstrated that an increase in the weight concentration from 0 to 2% resulted in a 27% enhancement in the oil recovery

factor, from 60 to 76%. Moreover, a pronounced impact of nanofluid was observed starting even from a nanoparticle concentration of 0.5 wt%.

Despite the recent proliferation of nanosuspensions research in the context of enhanced oil recovery, a number of unresolved issues in this field remain unanswered. In particular, there is no comprehensive understanding of the mechanisms of the influence of nanoparticle size and morphology on oil recovery during reservoir flooding. Most of the existing studies on the application of nanosuspensions for enhanced oil recovery are related to the use of spherical nanoparticles. In this paper, alumina nanofibers (ANF), which are a unique next-generation crystalline material with a high aspect ratio, are proposed for the first time as an additive for enhanced oil recovery. Alumina nanofiber suspensions may be a promising agent for enhanced oil recovery because they exhibit non-Newtonian properties at low concentrations [21]. To demonstrate the advantage of these nanosuspensions, a comparative analysis of the effects of alumina nanofibers and spherical silica nanoparticles on oil recovery during waterflooding was performed using microfluidic experiments. This is the first time such a study has been carried out.

2. Materials and Methods

This section describes the materials and methods used in the study. The basis of our work included the following steps. In the first stage, displacing agents were prepared, and their properties were determined (see Section 2.1). The nanomaterials used in the preparation are described in Section 2.1. The second stage was associated with conducting a microfluidic experiment; a detailed description is presented in Section 2.3. Section 3 analyzed the experimental results and determined the effect of adding nanomaterials on the displacement of oil from the porous chip.

2.1. Nanosuspensions

This work represents the first comparative microfluidic study of oil displacement efficiency using nanosuspensions with spherical particles and nanofibers. The effect of particle concentration under other equal conditions was also investigated. The SiO_2 suspensions with spherical particles were prepared by dilution of concentrated sol Ludox TM-50 in distilled water. Table 1 provides a brief description of the initial samples provided by the Sigma-Aldrich (St. Louis, MI, USA) manufacturer and used to prepare suspensions for further investigation. The initial suspensions were aqueous dispersions of silica. The average particle size was 22 nm, and the weight concentration was 50 wt%. The nanosuspensions under investigation were obtained by diluting the concentrated suspension with distilled water. The weight concentration of the study samples ranged from 0.125 to 2 wt%.

Table 1. Characteristics of source nanomaterials.

Sample	Packaging	Producer/City/ Country	Particle Shape	Diameter, nm	ζ-Potential, mV
Ludox TM-50	Sol	Sigma-Aldrich, St. Louis, USA	Spherical	22	−38
Al_2O_3	Powder	LLC Bardakhanov, Novosibirsk, Russia	Spherical	11	+35
Aluminan (ANF)	Powder	LLC Nanosynthesis, Krasnoyarsk, Russia	Nanofibers	8.7	+38

Powder of aluminum oxide spherical nanoparticles was purchased from LLC Bardakhanov. The specific surface area estimated by the BET method was 140 m^2/g. The average size calculated from the specific surface area was 11 nm.

Furthermore, aluminum oxide nanofibers (with the Aluminum trademark), obtained by a technology based on the oxidation of aluminum melt in a controlled gas environment, were used in this study. The resulting aluminum oxide nanofibers (γ-Al_2O_3) exhibit a uniaxially oriented array structure with weak bonding between adjacent nanofibers.

A comprehensive investigation of the characteristics of aqueous aluminum oxide nanofiber suspensions was conducted by the authors in a previous study [21].

In contrast to SiO_2 suspensions comprising spherical particles, which were obtained through a straightforward dilution process, suspensions of Al_2O_3 were produced by a specific technique. At the initial stage, Al_2O_3 powder samples were prepared in accordance with the above-specified percentages and subsequently placed in distilled water. This was followed by a two-stage homogenization process. At the initial stage, agglomerates were disrupted by stirring the solution in an OFITE 152-18 Prince Castle high-speed stirrer at 20,000 rpm for 30 min. The second step involved the ultrasonic treatment of colloidal solutions in a water bath for a period of 30 min using a Volna UZTA-0.4/22-OM brand ultrasonic apparatus. Consequently, stable suspensions with homogeneous distributions of nanoparticles were produced. The concentration of Al_2O_3 nanoparticles and nanofibers was also varied within the range of 0.125 to 2 wt%.

A series of electron microscopic studies were conducted employing a high-resolution FE-SEM Hitachi S-5500 scanning electron microscope. All electron images were captured in secondary electron (SE) mode at an accelerating voltage of 3 kV, a beam current of 10 μA, and a focal length of 100 to 200 μm. An illustrative example of electron microscopy data pertaining to Ludox TM-50 particles and ANFs is presented in Figure 1a. The results of the SEM analysis of the micrographs are consistent with the manufacturer's data on the average particle size (Table 1). Furthermore, the electron micrographs indicated that the nanoparticles in Ludox TM-50 suspensions exhibited a narrow nanoparticle size distribution. The morphology of the ANF (see Figure 1b) array was investigated by scanning electron microscopy (SEM) (Hitachi TM 4000, Japan) at an accelerating voltage of 15 kV and by transmission electron microscopy (TEM) Hitachi HT 7700 (Hitachi High-Tech, Tokyo, Japan) at an accelerating voltage of 40–300 kV [21]. Electron microscopy of aluminum oxide particles was performed using a JEM-2100 transmission electron microscope (JEOL, Tokyo, Japan). Aluminum oxide particles have a shape close to spherical (see Figure 1c).

One of the most significant properties of suspension is its viscosity. Viscosity plays a pivotal role in enhanced oil recovery in reservoir flooding applications. The higher the viscosity coefficient, the more effective the use of nanosuspension becomes. Consequently, the data on the viscosity coefficient of nanosuspension are of significant importance. The viscosity was measured utilizing a Brookfield DV2T rotational viscometer, which employs a calibrated spring to measure the twisting force exerted upon it as the spindle is rotated at a constant speed within the liquid under study. The Brookfield DV2T rotational viscometer allows one to study the viscosity–shear rate dependence. This is important for non-Newtonian media, such as nanofiber suspensions. The Brookfield DV2T viscometer is reported to have a stated error of ±2%, depending on the range used. Given that nanosuspensions frequently exhibit non-Newtonian properties, the present study employed a comprehensive approach to assess the dependence of viscosity coefficient on shear rate across the entire range of variation. The temperature was carefully controlled throughout the measurement process. All data presented below were obtained at 25 °C.

The viscosity coefficient of nanosuspensions with fibers exhibits a markedly different behavior. The dependence of the viscosity coefficient of nanosuspensions with ANF is illustrated in Figure 2. As can be observed, at nanofiber concentrations below 0.5 wt%, the viscosity of suspensions is independent of shear rate, and thus, suspensions are Newtonian. The viscosity coefficients in these cases are also provided in Table 2. It can be observed that even at low concentrations, the presence of fibers significantly increases the viscosity, with an increase of approximately 50% at a concentration of 0.25 wt%.

As illustrated in Figure 2, an increase in the ANF concentration results in the formation of non-Newtonian suspensions. The analysis of the dependence of the viscosity coefficient on the shear rate has demonstrated that the rheology of these suspensions is well described by a power law model $\eta = K\dot{\gamma}^{n-1}$, where K is the consistency index, Pa·s^n, $\dot{\gamma}$ is the shear

rate, s^{-1}, n is the flow behavior index. The data presented in Table 2 illustrate the dependence of rheological parameters (flow behavior index and consistency index) of suspensions with nanofibers. As the concentration of ANF increases, the flow behavior index decreases, and the consistency index increases. This suggests that the non-Newtonian properties are becoming more pronounced with an increase in the concentration of nanofibers.

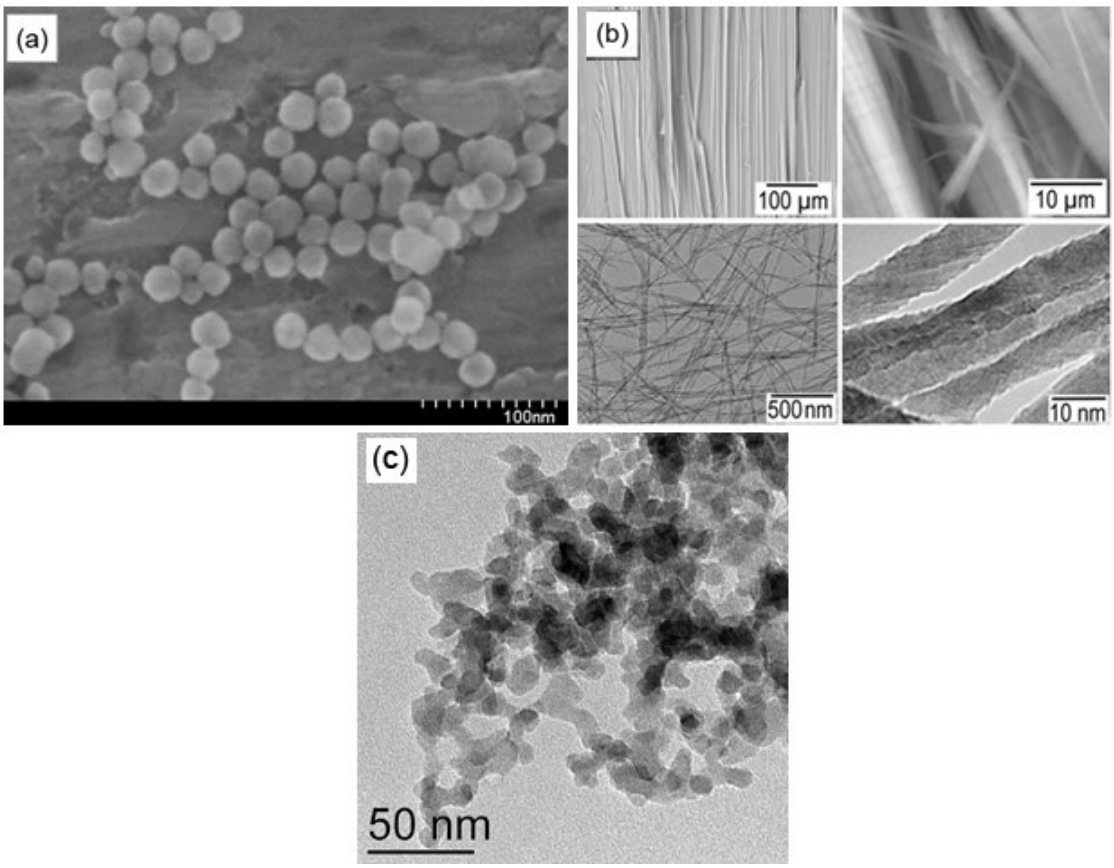

Figure 1. Electron microscopy of nanoparticles: (**a**) silica oxide nanoparticles (Ludox TM-50); (**b**) aluminum oxide nanofibers; and (**c**) aluminum oxide nanoparticles.

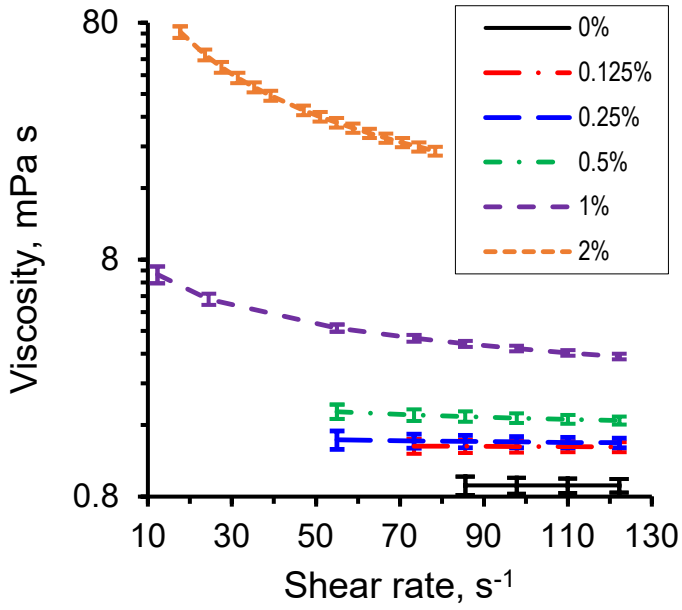

Figure 2. Dependence of viscosity of ANF suspension on shear rate.

Table 2. Physical properties of the displacement fluids used: water (W) and nanosuspensions.

Name	Concentration, wt%	Viscosity, mPa·s	Density, kg/m^3	Flow Behavior Index	Consistency Index, mPa·s^n
W	0	0.8909	997.0	-	-
0.125% Ludox	0.125	0.8933	997.7	-	-
0.25% Ludox	0.25	0.8963	998.4	-	-
0.5% Ludox	0.5	0.9024	999.7	-	-
1% Ludox	1	0.9147	1002	-	-
2% Ludox	2	0.9397	1008	-	-
0.125% Al_2O_3	0.125	0.8917	997.9	-	-
0.25% Al_2O_3	0.25	0.8929	998.8	-	-
0.5% Al_2O_3	0.5	0.8967	1001	-	-
1% Al_2O_3	1	0.9099	1004	-	-
2% Al_2O_3	2	0.9581	1011	-	-
0.125% ANF	0.125	1.307	997.9	-	-
0.25% ANF	0.25	1.378	998.8	-	-
0.5% ANF	0.5	-	1001	0.8909	2.824
1% ANF	1	-	1004	0.6539	16.45
2% ANF	2	-	1011	0.2234	679.5

Consequently, suspensions of spherical nanoparticles were identified as Newtonian fluids within the concentration range under consideration. The data on the viscosity of suspensions are presented in Table 2. It can be observed that the increment in the viscosity at the maximum concentration of SiO_2 and Al_2O_3 spherical nanoparticles in this case is relatively modest, amounting to approximately 5 and 7%, respectively. To date, the dependence of the viscosity of nanosuspensions on particle concentration has already been studied quite well. Furthermore, Table 2 presents the density of nanosuspensions. As can be observed, the density of the nanosuspensions differs insignificantly from that of water under the same conditions.

2.2. Oil

A crude oil sample with a density of 852 kg/m^3 and a viscosity of 17.8 mPa·s was employed in the experiments. The content of various organic and inorganic substances and their compounds was determined using Fourier transform infrared spectroscopy (FTIR). Oil mainly consists of aliphatic hydrocarbons of normal (unbranched) structure, contains a small number of aromatic structures, and oxygen- and sulfur-containing compounds.

2.3. Microfluidic Chip and Experimental Technique

In this study, a microfluidic chip (Part Number: 3200284, Dolomite Centre, Ltd., Royston, UK) was employed to simulate the porous structure of the rock (Figure 3). The chip material was B270 sodium lime glass. There is no channel coating; the glass is naturally hydrophilic. Hydrofluoric acid etching and thermal bonding methods were used to fabricate the microfluidic chip. Surface roughness of channels (Ra) was 5 nm.

The dimensions of the 4 mm thick microfluidic chip were 92.5 × 15.0 mm^2. The area of the porous region of the microchip was 10 × 60 mm^2 (see Figure 3a). The porous area was created by a 150-fold repetition of a 2 × 2 mm^2 square (Figure 3b). The channel arrangement in the square is a grid of 8 × 8 channels, which has an almost elliptical cross-section. The channel depth and width are 100 and 110 μm, respectively. The channels in the grid are characterized by randomly distributed constrictions, which simulate the natural structure of the rock. The grid contains 38 pores with a diameter of 63 μm, 40 pores with a diameter of 85 μm, and 50 straight channels.

A comprehensive description of the experiment is provided in [20]. The schematic diagram of the experimental setup is presented in Figure 4. The displacement fluid flow was regulated by means of a multi-channel, high-performance Elveflow OB1 MK3+ microfluidic pressure controller. The controller was equipped with two channels, each capa-

ble of maintaining pressure between 0 and 2 bar, and between 0 and 8 bar, respectively. For the second channel, the pressure maintenance accuracy was 100 Pa, the response time and pressure set time were up to 9 and 35 ms, respectively, and the minimum pressure increment was 24 Pa. The flow rate and differential pressure were monitored and controlled using the ESI program from Elveflow.

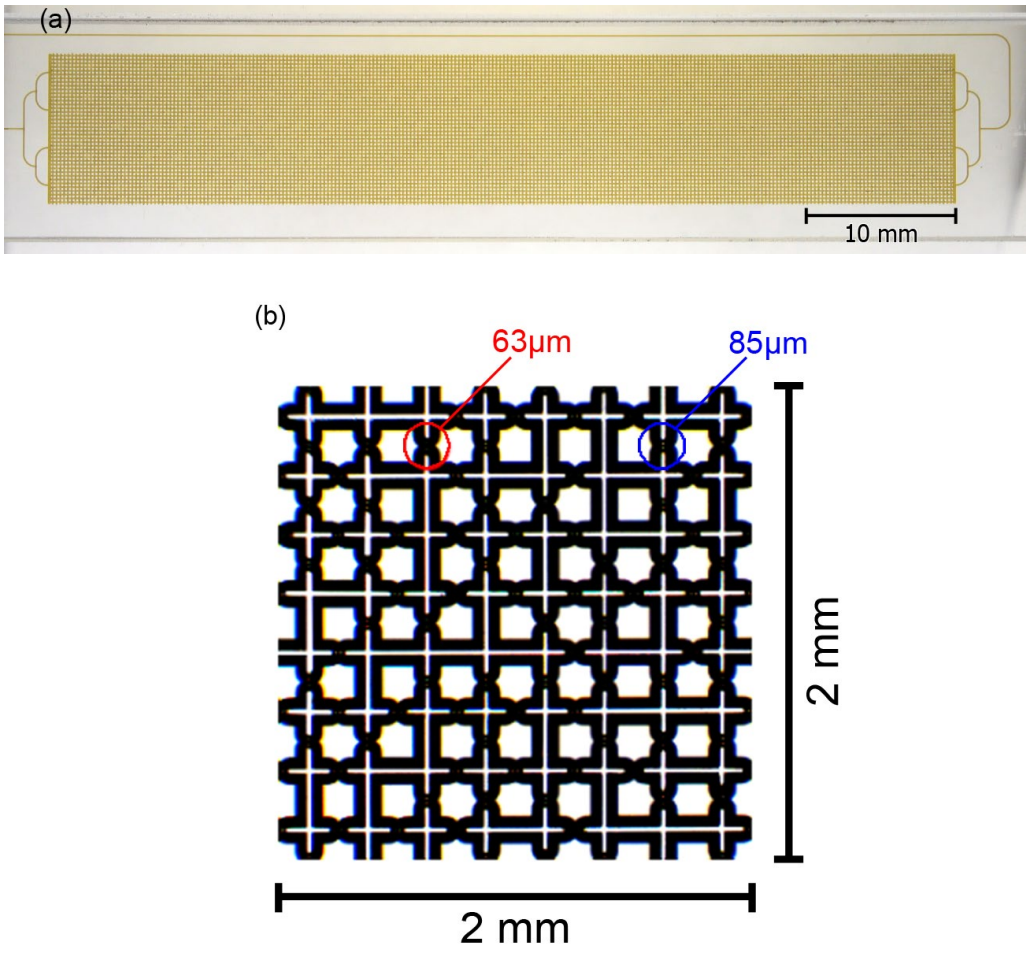

Figure 3. Microfluidic chip (**a**) and its enlarged fragment (**b**).

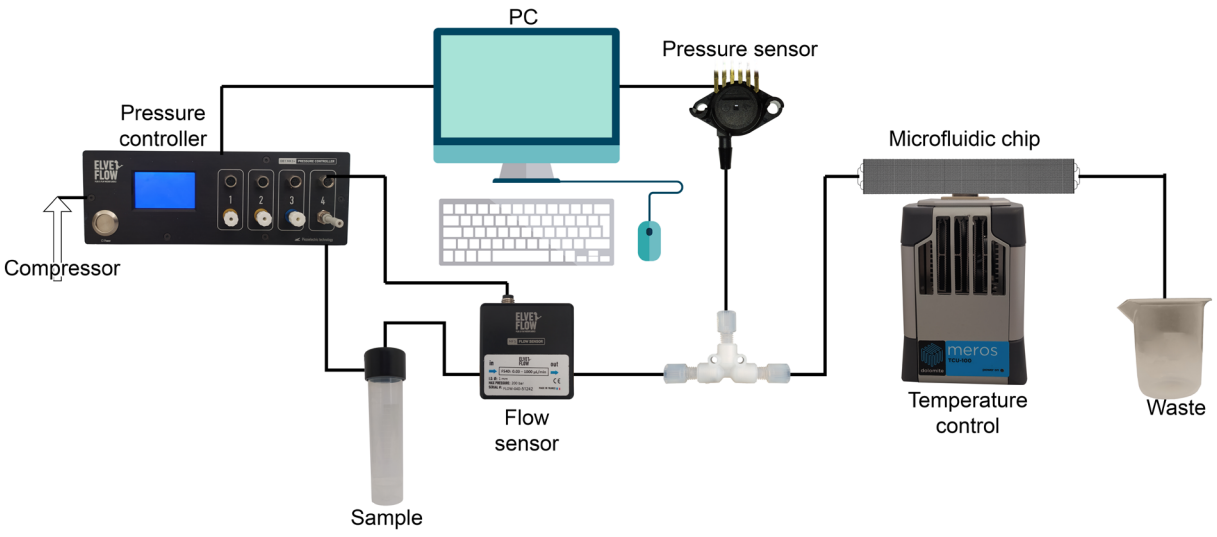

Figure 4. Schematic diagram of the experimental setup.

In order to operate, the controller requires an external pressure source, namely a compressor. The pressure controller directs compressed air into a sealed reservoir containing the displacement fluid under study. The microfluidic chip was connected to the reservoir via PTFE tubing with an outer diameter of 1/16 inch and placed horizontally. The temperature in the experiments was maintained constant at 25 °C using a TCU-100 microfluidic temperature control (Dolomite Microfluidics, Royston, UK). The temperature control of the microfluidic temperature controller ranged from 0 to 100 °C. The accuracy of temperature measurement was ±0.1 °C. The microfluidic chip was covered on the top with insulation to achieve more stable temperature conditions.

An MFS4 flow sensor was employed, operating within the range from 0.03 to 1000 µL/min with an accuracy of ±5% of the measured value. The sensor exhibited a response time of up to 70 ms. Calibration of the flow sensor was conducted by comparing the set flow rate on the pressure controller of the fluid (water) flowing during a given time interval with the flow rate calculated using the mass and density of the flowing fluid. The correction factor was calculated as the ratio of the set flow rate to the flow rate measured using the weights.

The pressure was recorded using an MPX5050GP relative pressure sensor with a measurement error of ±2.5%. The sensor's operating temperature ranged from −40 to +125 °C, and its operating pressure was up to 50 kPa.

The flow rate was set in microliters per minute (mL/min), and pressure versus time was recorded. For each specified flow rate, the mean pressure value was taken.

2.4. Experimental Procedure

Initially, the empty microchip was completely filled with oil. Thereafter, flooding with displacement fluid was implemented at a fixed flow rate. A number of pore volumes were pumped through. The flooding process was recorded by a high-speed camera, which subsequently saved the video for further analysis. The oil recovery factor, which is the ratio of the volume of displaced oil to the original volume, was estimated from photographs obtained during the experiment. The oil recovery factor was plotted in time using batch image processing. A comprehensive description of the software's operational details can be found in [20].

The microfluidic chip-washing procedure consists of several stages. After conducting an oil displacement experiment, the microfluidic chip is washed at a temperature of 100 °C. Syringe needle filters with a diameter of 25 mm and an aperture of 0.22 µm are used to prevent debris from entering the chip. The chip is first washed with distilled water to get rid of oil residues in the pores of the chip, then sequentially thoroughly washed with acetone, dichloroethane, isopropyl alcohol, and finally again with distilled water. After washing, the microfluidic chip is dried with air until moisture completely evaporates from the channel walls.

3. Research Results and Discussion

Initially, an experimental microfluidic water flooding was conducted. The microfluidic chip, which was completely filled with oil, was supplied with water at a volumetric flow rate of 0.5 µL/min. This corresponded to a capillary number of 8.4×10^{-6}. The dynamics of the oil displacement process with water is illustrated in the photographs in Figure 5. The direction of the water flow is from left to right. At the outset, the water traverses the microchip channels in a relatively uniform manner. The water movement front is nearly uniform. However, as the water advances, the flooding pattern changes. The water begins to move more actively along the edges of the microchip. The central region of the microchip remains occupied by oil. Moreover, a significant portion of the oil remains behind the displacement front in the form of individual islets as well as thin films at the walls of the microchannels.

Approximately 30 min after the commencement of the experiment, water begins to emerge from the microchip outlet and subsequently flows out through one of its outlets. Further, the water gradually reaches a steady state flow pattern as it continues to flow out

of the outlet. The final photograph in Figure 5 depicts the steady-state oil displacement pattern. Further, the water continues to flow through the channel formed at the upper edge of the microchip. The water flow channel at the lower edge of the microchip becomes a dead end, resulting in the cessation of flow along it.

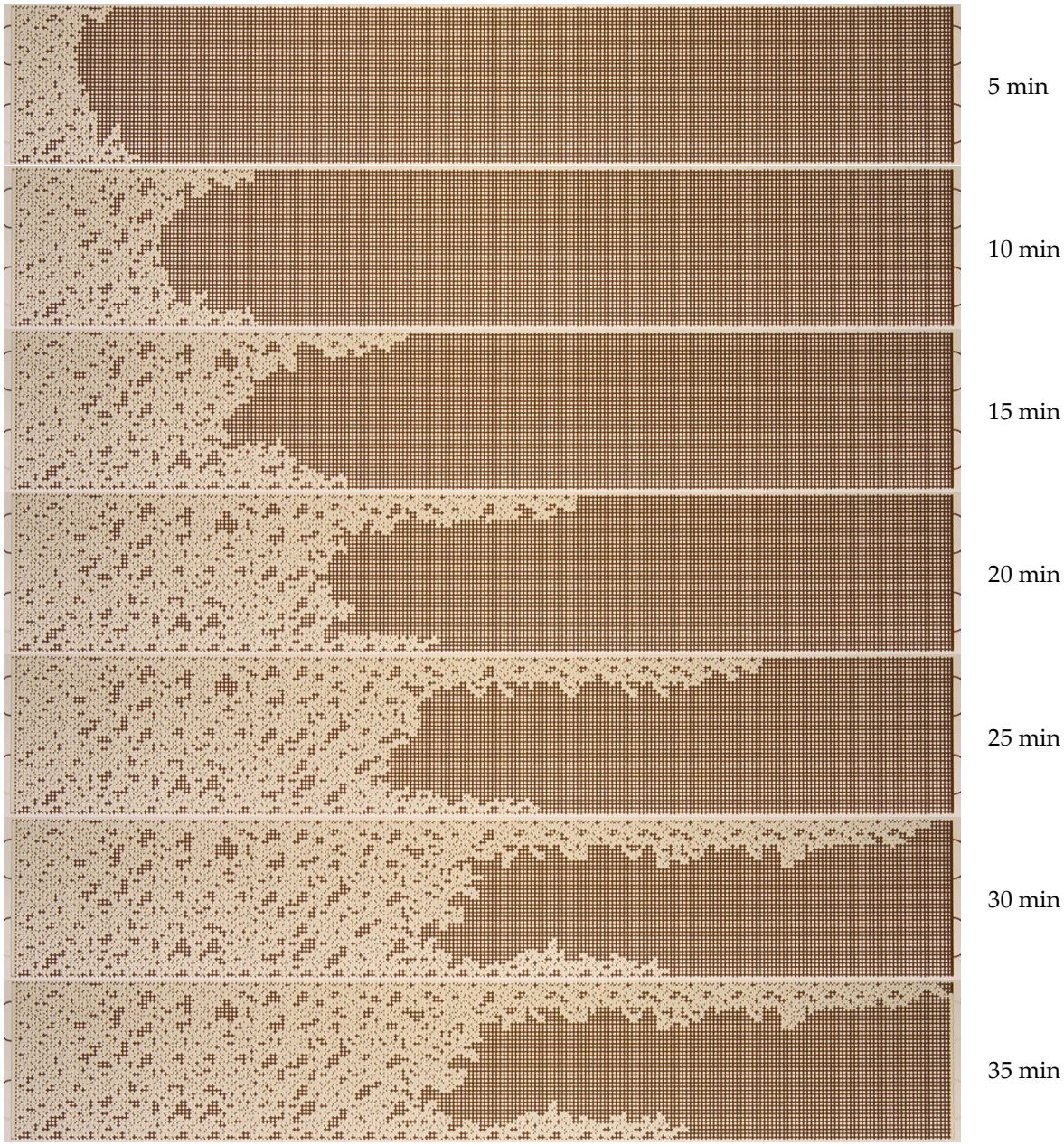

Figure 5. Photographs of the oil displacement by water. The water breakthrough at the outlet of the porous part of the microfluidic chip occurred at 31 min.

The oil recovery factor (ORF) was estimated using photographs obtained during the experiment. The ORF was defined as the proportion of residual oil in relation to its original volume. With regard to the microfluidic experiment, the ORF was calculated by determining the fraction of pixels in the photographs that exhibited color saturation levels corresponding to oil. As a result, the ORF for the microfluidic chip when displaced by water was 44%. Initially, the ORF exhibited a linear correlation with time. This can be interpreted as essentially representing the mass conservation law when filling a fixed volume with

two different media. Subsequently, upon the water reaching the microchip outlet, the ORF stabilizes, as previously mentioned.

Further, a series of microfluidic oil displacement experiments were conducted using suspensions of spherical silicon oxide nanoparticles with an average size of 22 nm (Ludox TM-50, Sigma Aldrich). The flow rate of the suspensions during the displacement process was identical to that in experiments with water, equaling 0.5 μL/min. The oil displacement dynamics from the microchip by nanosuspension with a particle concentration of 2 wt% are illustrated in Figure 6. A comparison of Figures 5 and 6 reveals a change in the character of the interface front movement. The flow of nanoparticle suspensions occurs in the form of separate jets, similar to those observed when displacing oil with water. However, the width of these jets increases significantly (Figure 6). Moreover, the channels through which the nanosuspension flows encompass a greater proportion of the microchip volume. In contrast to the predominantly walls-directed flow of water, the nanosuspension course beds exhibit more complex trajectories in the microchip volume. This results in the central area occupied by oil (see Figure 5) being broken into several separate islets, which are streamlined by the nanosuspension. As a result, the nanosuspension flow encompasses the majority of the channels within the microchip model. This results in an increase in the ORF from 44% at water displacement to 53% at displacement by Ludox TM-50 suspensions with a particle concentration of 2 wt%. Another significant distinction between displacements by nanosuspension is the increase in breakthrough time to the microchannel model outlets. Since the nanosuspension flows through the pore space of the microchip in more tortuous channels, this results in a later breakthrough to the microchip outlet. As illustrated in Figures 5 and 6, the nanosuspension takes approximately 30 min to reach the microchannel outlet, while at Ludox concentrations above 0.5%, the breakthrough time increases to approximately 35 min.

Figure 7 illustrates the residual oil distribution in a microfluidic chip following displacement by nanosuspensions comprising varying concentrations of spherical silicon oxide particles. The results of microfluidic experiments on oil displacement with Ludox TM-50 suspension have demonstrated that their application resulted in an increase in the ORF at concentrations exceeding 0.5 wt%. Thus, it was determined that at a solution concentration of 0.5%, the ORF was 43%, while at the maximum concentration, it was 53%. Concurrently, when utilizing water, the ORF was 44%, as reported previously. The displacement patterns (Figure 7) indicate that at low concentrations of nanoparticles, the movement of the displacement front and the character of residual oil distribution are similar to those observed during oil displacement with water. The above-described flow peculiarities emerge when the concentration of particles exceeds 0.5 wt%. As a result, in the microfluidic microchip, the size of the zones filled with oil decreases with increasing particle concentration. The quantitative data on the effect of spherical particle concentration is presented in Figure 8. Upon increasing the nanoparticle concentration to 1–2 wt%, an increase of approximately 9% was observed in the ORF compared to water. Our recent work [20] examined the application of Ludox TM-50 suspension to displace more viscous oil at high flow rates (45 μL/min). It was demonstrated that ORF exhibited a monotonic increase with increasing nanoparticle concentration, rising from approximately 60 to 76% at a concentration of 2 wt%. In this study, we have considered the case in which the capillary number at displacement was more than 100 times smaller. This resulted in a significant reduction in the ORF. Nevertheless, the impact of nanoparticle additive persisted, albeit at a diminished level, and the concentration threshold at which this impact became apparent increased.

The potential impact of nanoparticles on oil displacement efficiency has been investigated previously [22]. Our findings indicate that with increasing nanoparticle concentration, the interfacial tension coefficient declines notably, accompanied by a change in wettability with respect to oil. The surface becomes hydrophobic. In particular, for Ludox TM-50 (22 nm) nanosuspension, it has been demonstrated that the wetting angle at the oil–water–rock interface increases from 73 to 153° when the concentration of nanoparticles increases

from 0 to 2 wt%. This means that the surface is transformed from water-wettable to oil-wettable. Moreover, the interfacial tension of the Ludox TM-50 nanosuspension decreases by approximately 50% in comparison to water as the nanoparticle concentration increases. This results in enhanced oil washing off solid surfaces and improved washout of oil, which undoubtedly impacts the oil recovery factor during flooding with nanosuspension. As illustrated in Table 2, the viscosity of the SiO_2-containing nanosuspension is not appreciably different from that of water (approximately 5% higher). This increase in viscosity is insufficient to account for the observed 9% increase in ORF. Consequently, the primary factor contributing to the observed increase in ORF is the impact of suspension on wettability and interfacial tension.

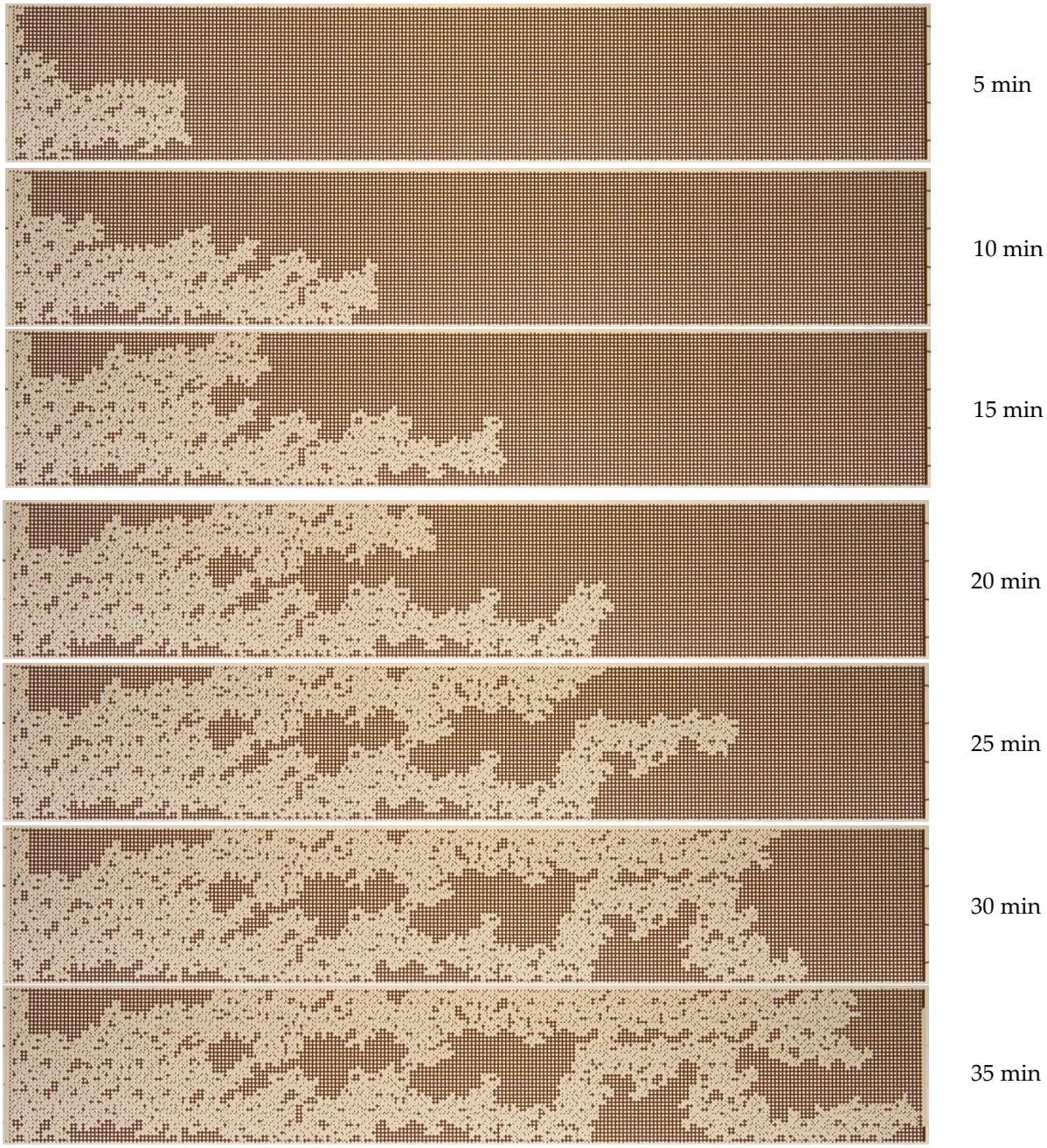

Figure 6. Photographs of oil displacement process with Ludox TM-50 nanosuspension at a concentration of 2 wt%. The breakthrough of 2% Ludox TM-50 suspension at the outlet of the porous part of the microfluidic chip was at 34 min.

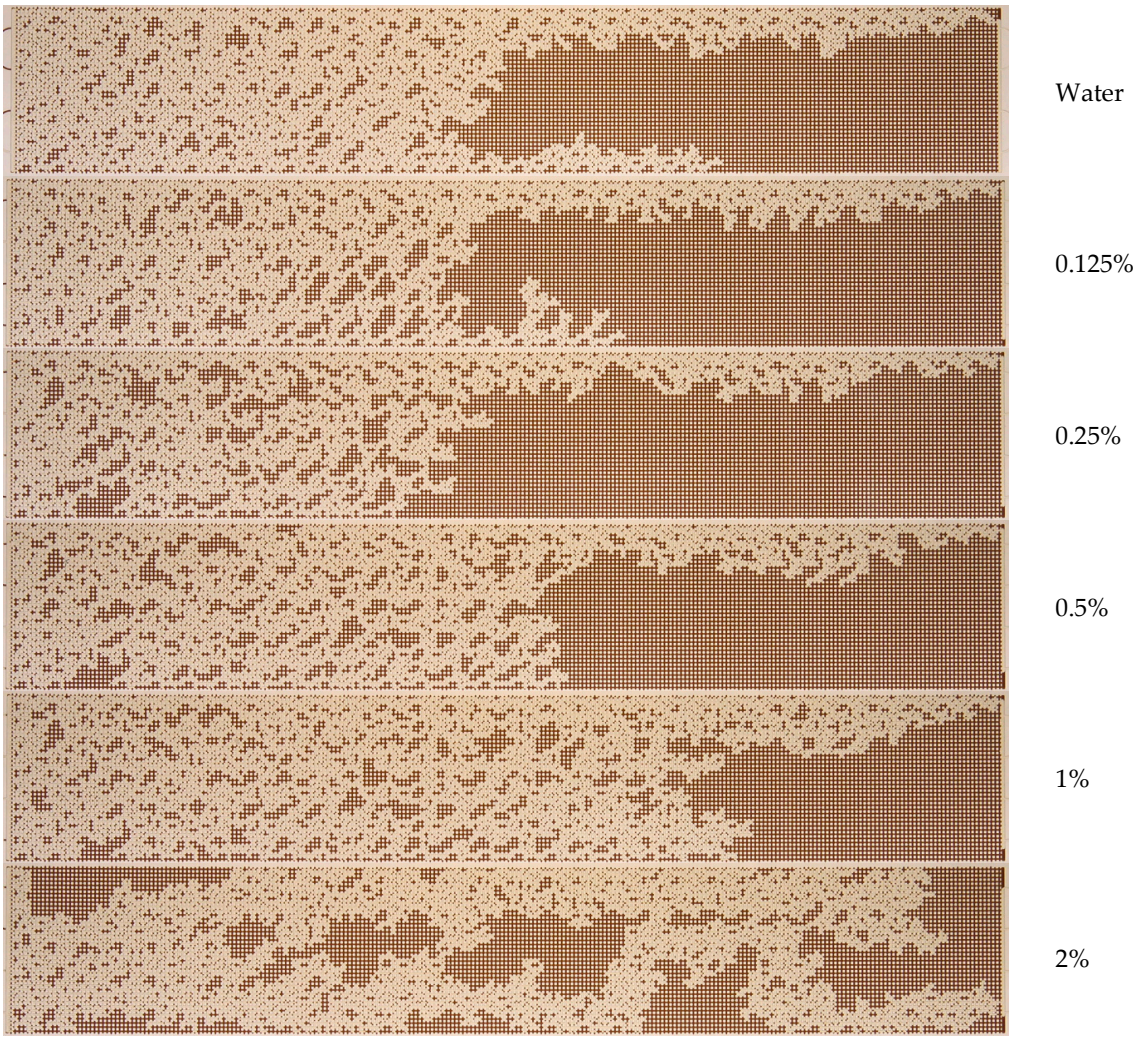

Figure 7. Final photographs of residual oil after pumping through Ludox TM-50 suspension with different particle concentrations.

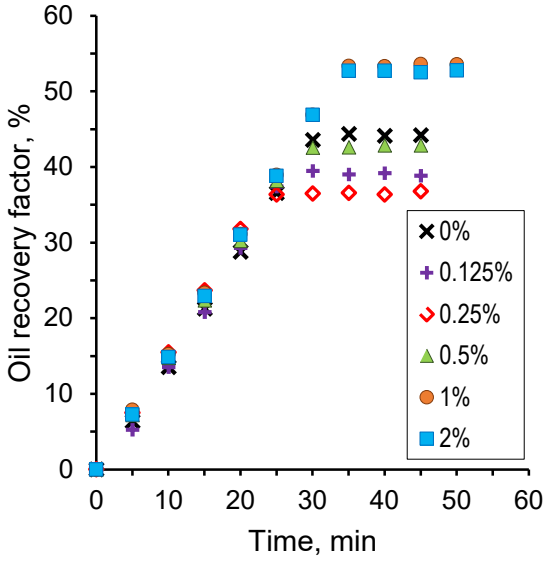

Figure 8. Dependence of oil recovery factor on time during displacement by SiO_2 nanosuspension (22 nm) with different particle concentrations.

Furthermore, similar experiments were conducted on the displacement of an oil sample by the suspension of aluminum oxide nanofiber. In contrast to the use of suspensions containing spherical nanoparticles, microfluidic studies with nanofibers were performed for the first time exactly in the present work. The flow rate of the suspension was 0.5 μL/min. The main results are presented in Figures 9 and 10. Figure 9 presents photographs of the final oil distribution within the microfluidic chip following displacement by a suspension comprising varying concentrations of aluminum oxide nanofibers. Figure 10 illustrates the temporal evolution of the ORF for distinct nanofiber concentrations. The analysis of the photographs of the residual oil fraction distribution indicates that a notable enhancement in oil displacement is observed at nanofiber concentrations exceeding 0.5%. As the concentration of ANF increases, the efficiency of oil displacement also increases. This is obvious from the figure, which illustrates that as the ANF concentration increases, the size of the central zone in the microchip occupied by oil decreases monotonically. At an ANF concentration of 1–2%, this zone effectively disappears. At concentrations of 1–2%, the movement of displacement front becomes near-uniform. As a result, residual oil persists in the form of small islets distributed uniformly throughout the microchip, situated behind the displacement front. Movement of the displacement front at high nanofiber concentrations becomes more uniform, resulting in a notable increase in the breakthrough time of the nanosuspension to the microchip outlet. Thus, Figure 10 illustrates that the breakthrough time increases from 30 to 50 min with increasing the ANF concentration. Certainly, this has a beneficial effect on the quality of oil displacement, which is enhanced significantly. Consequently, the incorporation of 2 wt% nanofibers has been observed to elevate the ORF by approximately 25%. However, in this case, the optimal nanofiber concentration is 1 wt%. The increase in ORF for this additive at noted concentration is approximately 21%, which is more rational for the application of this nanosuspension in reservoir flooding of oilfields.

Similar experiments to avoid different results due to differences in material properties. Experiments on oil displacement from a microfluidic chip using a suspension of spherical Al_2O_3 nanoparticles (11 nm) were conducted. Figure 11 presents photographs of the final distribution of oil and Al_2O_3 suspension with different concentrations of spherical nanoparticles. Figure 12 shows the dependencies of the oil recovery factor during displacement using Al_2O_3 suspension with different spherical particle concentrations.

The oil displacement process changes when the porous structure of the microfluidic chip is flooded with a nanosuspension. Figure 5 shows the movement of the front of oil displacement by water, which occurs in the form of individual jets (“viscous fingers”). The final distribution of oil and suspension at different concentrations of nanoparticles and nanofibers is different (see Figures 7, 9 and 11). The dependence of the breakthrough time on the concentration of nanoparticles and nanofibers is shown in Figure 13a. This dependence is non-monotonic. At low concentrations (less than 0.25%), a decrease in the breakthrough time of the suspension is observed. With an increase in concentration above 0.5%, the displacement front becomes more uniform, and the width of the jets increases, covering a larger area. As a result, the breakthrough of the displacing fluid to the outlet of the microporous medium occurs significantly later. The breakthrough time increases with an increase in the concentration of nanoparticles. Thus, at the maximum considered concentration of Ludox TM-50 nanoparticles, the breakthrough time increased by 10% compared to water displacement. When flooding with ANF suspension, the displacement front is more uniform (see Figure 9). The breakthrough time of the suspension at concentrations above 0.5% increases by 50% compared to water flooding. At comparable concentrations, the breakthrough time was longer for alumina nanofibers. It was found that the shorter the breakthrough time, the lower the oil recovery factor. This means that at a fixed injection rate, the volume of coverage of the porous medium by the nanofluid increases by approximately the same amount. This certainly leads to a significant increase in oil displacement.

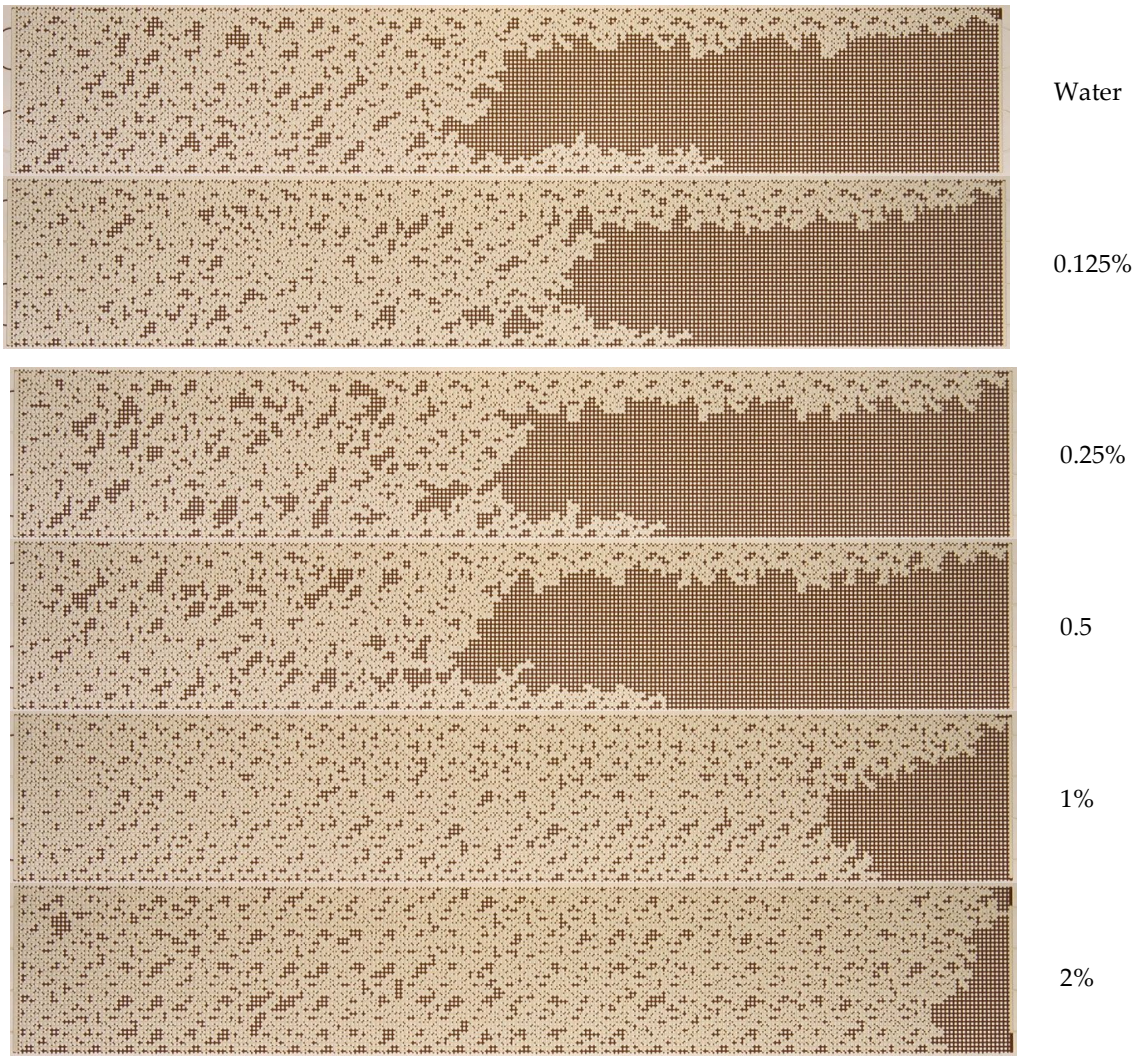

Figure 9. Final photographs of residual oil after pumping ANF suspension with different particle concentrations.

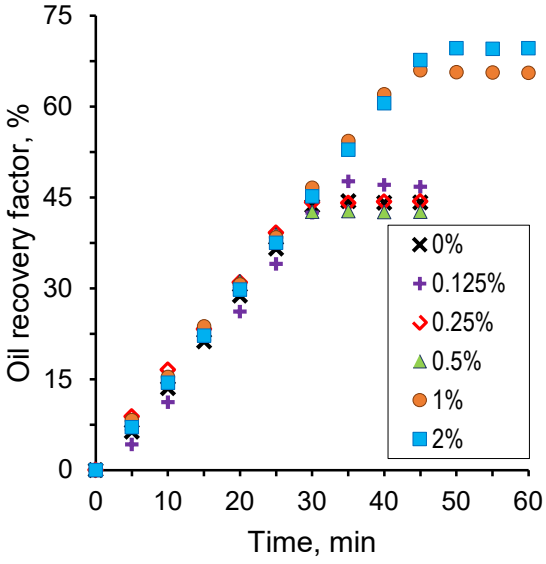

Figure 10. Dependence of oil recovery factor on time during displacement by ANF suspension with different nanofiber concentrations.

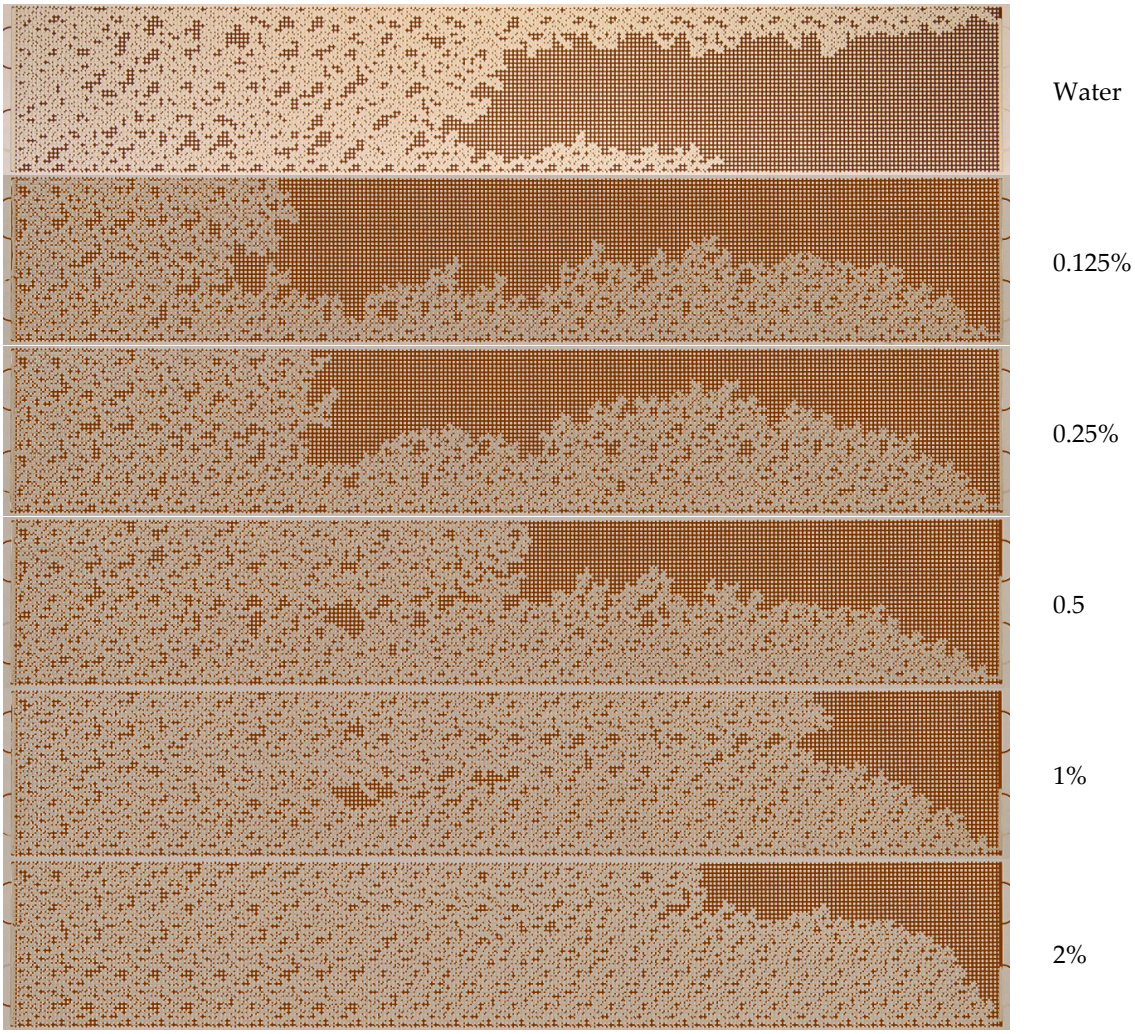

Figure 11. Final photographs of residual oil after pumping Al_2O_3 suspension with different particle concentrations.

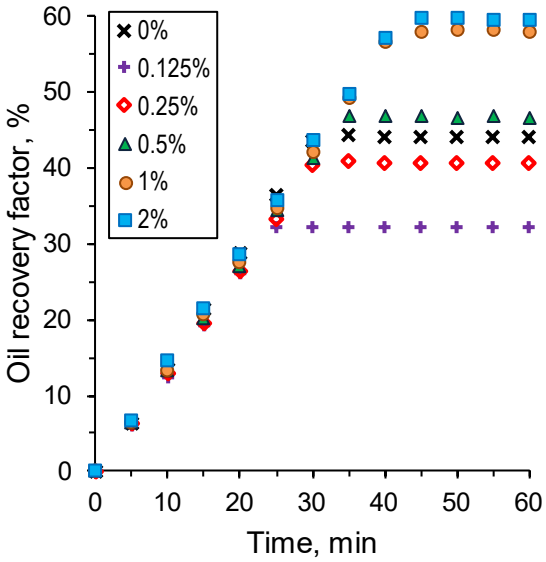

Figure 12. Dependence of oil recovery factor on time during displacement by Al_2O_3 suspension (11 nm) with different particle concentrations.

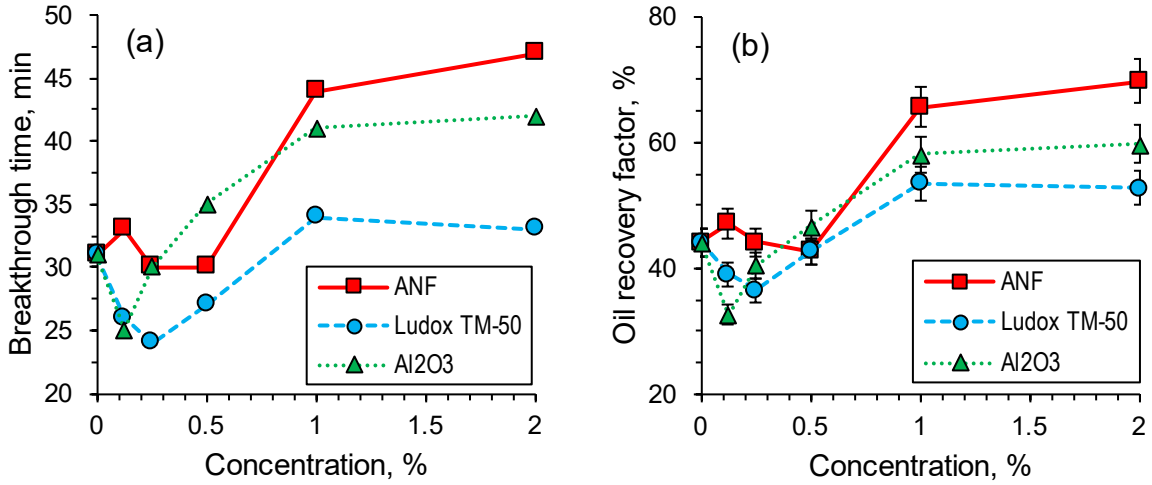

Figure 13. Dependence of breakthrough time (**a**) oil recovery factor (**b**) on the concentration of particles.

The dependence of oil displacement from the microchip on the concentration of spherical nanoparticles and nanofibers is presented in Figure 13b. As can be observed, the use of elongated nanofibers is more effective for oil displacement, provided that all other conditions are equal. The application of nanofibers allows for the maximum increment of ORF to be reached at a level of 25%, while the application of spherical nanoparticles allows for reaching the maximum increment of ORF at a level of 10%.

A quantitative analysis of the dependence of ORF on concentration reveals a sharp increase in ORF with increasing nanofiber concentration above 0.5 wt%. From the data presented in Figure 2 and Table 2, it can be observed that at these concentrations, the nanosuspension becomes non-Newtonian. As the concentration of ANF increases, the flow behavior index decreases, and the consistency index increases. This behavior can be explained by the particle size in suspensions, which is of great importance. Nanofibers, due to their high aspect ratio (L/D > 58), are characterized by a low percolation threshold, which has a stronger effect on rheological properties than spherical nanoparticles at comparable concentrations. It is a well-known fact that when the flow behavior index of a non-Newtonian fluid decreases, the velocity profile of the fluid flattens as it flows in the channel. The velocity profile becomes flatter. At a fixed flow rate, the flattening of the velocity profile results in a local increase in velocity near the channel walls, which locally contributes to better oil displacement. Furthermore, the effective viscosity of the non-Newtonian suspension increases by several orders of magnitude and exceeds the viscosity of oil, which undoubtedly contributes to its better displacement. It was demonstrated that the primary mechanism responsible for enhanced oil displacement during reservoir flooding of nanofiber suspensions is their non-Newtonian behavior. In fact, nanosuspensions of aluminum oxide nanofibers at concentrations above 0.5% exhibit an oil displacement mechanism that is similar to non-Newtonian solutions of polymers, which are also commonly utilized for reservoir flooding in various oil fields. However, in contrast to polymer solutions, which are susceptible to degradation, nanosuspensions are characterized by their absolute thermal and biological stability. This renders them a promising candidate for application in enhanced oil recovery.

4. Conclusions

Microfluidic studies of oil displacement processes using nanosuspensions of different morphology have been conducted. For this purpose, nanosuspensions containing silicon oxide spherical particles (22 nm), aluminum oxide spherical particles (11 nm), and aluminum oxide nanofibers (with a diameter of 8.7 ± 2.4 nm and an aspect ratio of L/D~58) were used. The study of ANF-containing nanosuspensions in oil recovery processes was conducted for the first time ever. The impact of nanoparticles with varying shapes and

concentrations (ranging from 0.125 to 2 wt%) on the characteristics of nanosuspensions was investigated. A comparative analysis has revealed that the incorporation of nanofibers resulted in a considerably greater enhancement of oil recovery factor (ORF) in comparison to the addition of spherical nanoparticles, provided that all other conditions remained equal. In particular, it was demonstrated that the utilization of nanofibers allows attaining the maximum enhancement of ORF up to 25%, while the use of spherical nanoparticles allows for the maximum increase in ORF to be no more than 10%. This is due to the fact that nanofiber additives not only alter the surface wettability but also exert a profound influence on the viscosity of nanosuspensions.

It should be noted that the particle size in suspensions is of great importance. Nanofibers, due to their high aspect ratio (L/D > 58), are characterized by a low percolation threshold, which has a stronger effect on rheological properties than spherical nanoparticles at comparable concentrations. It has been demonstrated that the incorporation of nanofibers exerts a tenfold greater effect on the viscosity of suspensions relative to analogous additions of spherical particles. The non-Newtonian behavior of ANF suspensions was observed at a weight concentration of 0.5 wt% and higher. This behavior represents the primary mechanism responsible for the observed increase in oil recovery factor following the injection of aluminum oxide nanofiber containing nanosuspensions. The results of microfluidic experiments have demonstrated that the novel ANF material is a promising candidate for addressing the challenges of enhanced oil recovery. A study of the effect of particle material on improving oil recovery using microfluidic technologies would be interesting. There are no works related to the use of silica nanorod suspensions, but there are enough studies of silica spherical nanoparticle suspensions. Therefore, further studies in this area are worthwhile and should be continued. However, a serious issue remains to be resolved regarding the preparation of nanosuspensions in the field. In laboratory conditions, the use of ultrasonic dispersion has proven very effective for the preparation of stable suspensions with nanofibers. In the field, the use of ultrasonic treatment is possible, but this will require the development of special equipment.

Author Contributions: Conceptualization, A.P. and A.M.; methodology, A.P.; formal analysis, A.P.; investigation, A.P. and V.Z.; resources, V.Z.; writing—original draft preparation, A.P., M.P., V.Z. and A.M.; writing—review and editing, A.P., M.P. and A.M.; visualization, A.P.; supervision, M.P. and A.M.; project administration, A.M.; funding acquisition, A.M. All authors have read and agreed to the published version of the manuscript.

Funding: This research was funded by the Ministry of Science and Higher Education of the Russian Federation, grant number FSRZ-2020-0012.

Data Availability Statement: Dataset available on request from the authors.

Acknowledgments: The authors also thank M. M. Simunin and A. S. Voronin for providing samples of aluminum oxide nanofibers.

Conflicts of Interest: The authors declare no conflicts of interest.

References

1. Shah, A.; Fishwick, R.; Wood, J.; Leeke, G.; Rigby, S.; Greaves, M. A review of novel techniques for heavy oil and bitumen extraction and upgrading. *Energy Environ. Sci.* **2010**, *3*, 700–714. [CrossRef]
2. Sun, C.; Guo, H.; Li, Y.; Song, K. Recent Advances of Surfactant-Polymer (SP) Flooding Enhanced Oil Recovery Field Tests in China. *Geofluids* **2020**, *2020*, 8286706. [CrossRef]
3. Watson, A.; Trahan, G.A.; Sorensen, W. An Interim Case Study of an Alkaline-Surfactant-Polymer Flood in the Mooney Field, Alberta, Canada. In Proceedings of the SPE Improved Oil Recovery Symposium, Tulsa, OK, USA, 12–16 April 2014. [CrossRef]
4. Lifton, V.A. Microfluidics: An enabling screening technology for enhanced oil recovery (EOR). *Lab Chip* **2016**, *16*, 1777–1796. [CrossRef] [PubMed]
5. Saadat, M.; Yang, J.; Dudek, M.; Øye, G.; Tsai, P.A. Microfluidic investigation of enhanced oil recovery: The effect of aqueous floods and network wettability. *J. Pet. Sci. Eng.* **2021**, *203*, 108647. [CrossRef]
6. Gao, W.; Li, Y.; Zhang, J.; Luan, H.; Cao, H.; Yu, Z. Effect of surfactant on pore-scale mobilization characteristics in various pore structure conglomerate for enhanced oil recovery. *Colloids Surf. A Physicochem. Eng. Asp.* **2021**, *627*, 127150. [CrossRef]

7. Eltoum, H.; Yang, Y.-L.; Hou, J.-R. The effect of nanoparticles on reservoir wettability alteration: A critical review. *Pet. Sci.* **2020**, *18*, 136–153. [CrossRef]
8. Mullayanov, A.I.; Pityuk, Y.A. Estimation of the Efficiency of Oil Displacement by a Micellar Solution with Addition of Nanoparticles Based on a Bulk Model of Porous Medium. *Fluid Dyn.* **2023**, *58*, 406–412. [CrossRef]
9. Mullayanov, A.I.; Pityuk, Y.A.; Safargalieva, E.M. Displacement of oil by micellar solution with nanoparticles from porous model with core material. *Pet. Eng.* **2024**, *22*, 45–55. [CrossRef]
10. Gilaev, G.G.; Amer, M.; Al-Idrisi, M.S. Application of nanotechnology for enhanced oil recovery: Nanofluids. *Constr. Oil Gas Wells Onshore Offshore* **2023**, *11*, 42–49.
11. Tuok, L.P.; Elkady, M.; Zkria, A.; Yoshitake, T.; Nour Eldemerdash, U. Evaluation of stability and functionality of zinc oxide nanofluids for enhanced oil recovery. *Micro Nano Syst. Lett.* **2023**, *11*, 12. [CrossRef]
12. Isaac, O.T.; Pu, H.; Oni, B.A.; Samson, F.A. Surfactants employed in conventional and unconventional reservoirs for enhanced oil recovery—A review. *Energy Rep.* **2022**, *8*, 2806–2830. [CrossRef]
13. Hadia, N.J.; Ng, Y.H.; Stubbs, L.P.; Torsæter, O. High Salinity and High Temperature Stable Colloidal Silica Nanoparticles with Wettability Alteration Ability for EOR Applications. *Nanomaterials* **2021**, *11*, 707. [CrossRef] [PubMed]
14. Li, D.; Wang, Y.; Liang, S.; Bai, B.; Zhang, C.; Xu, N. Synthesizing dendritic mesoporous silica nanoparticles to stabilize Pickering emulsions at high salinity and temperature reservoirs. *Colloids Surf. A Physicochem. Eng. Asp.* **2024**, *687*, 133481. [CrossRef]
15. Li, S.; Ng, Y.H.; Lau, H.C.; Torsæter, O.; Stubbs, L.P. Experimental Investigation of Stability of Silica Nanoparticles at Reservoir Conditions for Enhanced Oil-Recovery Applications. *Nanomaterials* **2020**, *10*, 1522. [CrossRef] [PubMed]
16. Maurya, N.K.; Mandal, A. Investigation of synergistic effect of nanoparticle and surfactant in macro emulsion based EOR application in oil reservoirs. *Chem. Eng. Res. Des.* **2018**, *132*, 370–384. [CrossRef]
17. Almahfood, M.; Bai, B. The synergistic effects of nanoparticle-surfactant nanofluids in EOR applications. *J. Pet. Sci. Eng.* **2018**, *171*, 196–210. [CrossRef]
18. Yekeen, N.; Padmanabhan, E.; Idris, A.K.; Ibad, S.M. Surfactant adsorption behaviors onto shale from Malaysian formations: Influence of silicon dioxide nanoparticles, surfactant type, temperature, salinity and shale lithology. *J. Pet. Sci. Eng.* **2019**, *179*, 841–854. [CrossRef]
19. Betancur, S.; Olmos, C.M.; Pérez, M.; Lerner, B.; Franco, C.A.; Riazi, M.; Gallego, J.; Carrasco-Marín, F.; Cortés, F.B. A microfluidic study to investigate the effect of magnetic iron core-carbon shell nanoparticles on displacement mechanisms of crude oil for chemical enhanced oil recovery. *J. Pet. Sci. Eng.* **2020**, *184*, 106589. [CrossRef]
20. Pryazhnikov, M.I.; Minakov, A.V.; Pryazhnikov, A.I.; Denisov, I.A.; Yakimov, A.S. Microfluidic Study of the Effect of Nanosuspensions on Enhanced Oil Recovery. *Nanomaterials* **2022**, *12*, 520. [CrossRef]
21. Minakov, A.V.; Pryazhnikov, M.I.; Simunin, M.M.; Dobrosmyslov, S.S.; Kuular, A.A.; Molokeev, M.S.; Volochaev, M.N.; Khartov, S.V.; Voronin, A.S. Rheological properties of colloidal suspensions of alumina nanofibers. *J. Mol. Liq.* **2022**, *367*, 120385. [CrossRef]
22. Minakov, A.V.; Pryazhnikov, M.I.; Suleymana, Y.N.; Meshkova, V.D.; Guzei, D.V. Experimental study of nanoparticle size and material effect on the oil wettability characteristics of various rock types. *J. Mol. Liq.* **2021**, *327*, 114906. [CrossRef]

Disclaimer/Publisher's Note: The statements, opinions and data contained in all publications are solely those of the individual author(s) and contributor(s) and not of MDPI and/or the editor(s). MDPI and/or the editor(s) disclaim responsibility for any injury to people or property resulting from any ideas, methods, instructions or products referred to in the content.